Figures

Table 1. The nine precipitation datasets used in Guirguis and Avissar (2007a) and (2007b).

Dataset	Spatial Resolution	Temporal Domain	Data Source
GPCC[a]	2.5° x 2.5°	From 1979	Raingauge
GPCP[b]	2.5° x 2.5°	From 1979	Raingauge, satalite
CMAP[c]	2.5° x 2.5°	From 1979	Raingauge,satellite
NCEP2[d]	210 km x 210 km	From 1979	Reanalysis
NARR[e]	32km x 32km	From 1979	Reanalysis
USMex[f]	1° x 1°	From1948	Raingauge
PriMet[g]	1° x 1°	1948-2000	Reanalysis
VIC[h]	1/8° x 1/8°	1950-2000	Raingauge with orographic adjustment
PRISM[i]	4km x 4km	From 1890	Raingauge with orographic adjustment

[a]Global Precipitation Climatology Center (GPCC) Monitoring Product (Rudolf and Schneider, 2005; Fuchs and Schneider, 2007)
[b]Global Precipitation Climatology Project (GPCP) version 2 Combined Precipitation Dataset (Huffman et al., 1997)
[c]CPC Merged Analysis of Precipitation (CMAP) (Xie and Arkin, 1997)
[d]NCEP-DOE Reanalysis-2 (Kanamitsu et al., 1996)
[e]North American Regional Reanalysis (Mesinger et al., 2004)
[f]CPC retrospective United States and Mexico daily precipitation analysis (Higgins et al., 2000)
[g]Global Meteorological Forcing Dataset for land surface modeling (Sheffield et al., 2004)
[h]VIC Retrospective Land Surface Dataset (Maurer et al., 2002)
[i]Parameter-elevation Regressions on Independent Slopes Model (Daly et al., 1994)

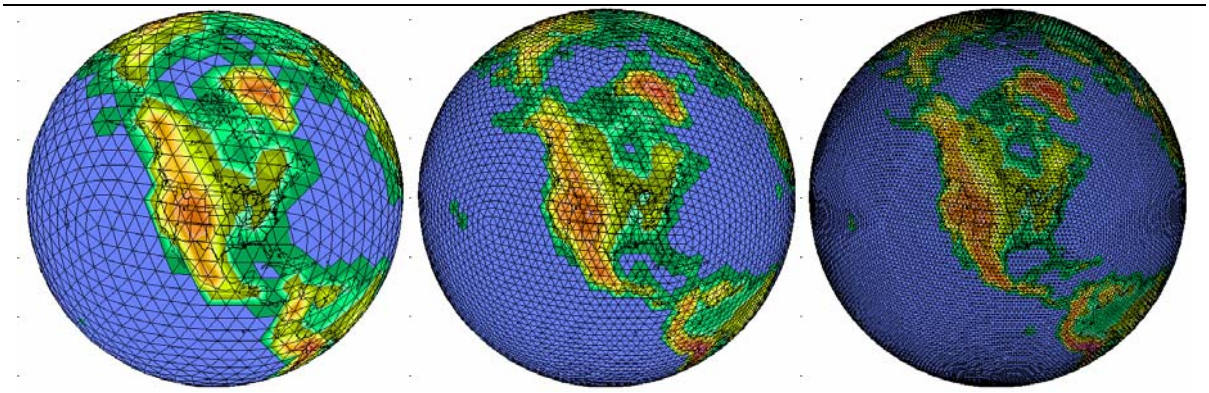

Figure 1. OLAM grid configuration for a horizontal CLS of 4º, 2º, and 1º. The data field plotted is topography.

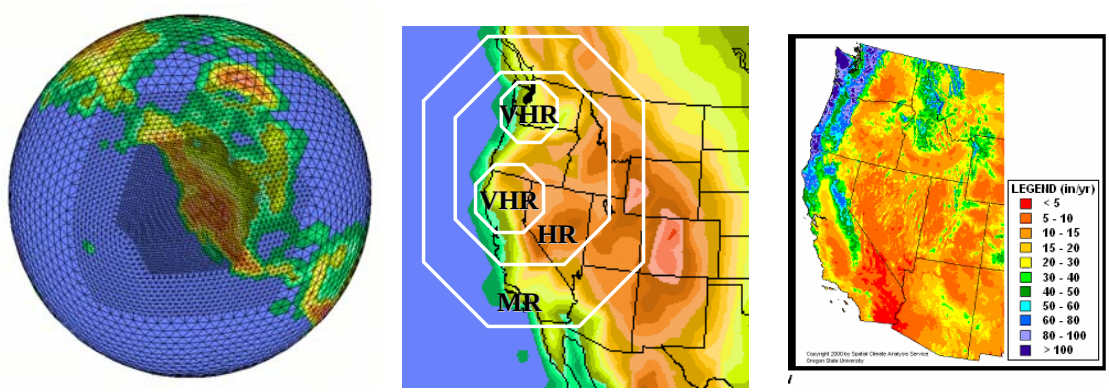

Figure 2. *Left:* OLAM grid showing three grid refinement levels (CLF of 2.5°, 1.3° and 0.6°), *Center:* Diagram of the refined grid configuration illustrating the approximate positions of the very-high resolution (VHR), high resolution (HR), and medium resolution (MR) grids. Here VHR, HR, and MR correspond to a CLS of 1-km, 4-km, and 8 km, respectively (note that there will be a transitionary 2-km refinement level between the VHR and HR levels due to the 2:1 grid refinement ratio). *Right:* Average annual precipitation as simulated by Christopher Daly using PRISM (based on 1961-1990 normals from NOAA stations & NRCS SNOTEL sites).

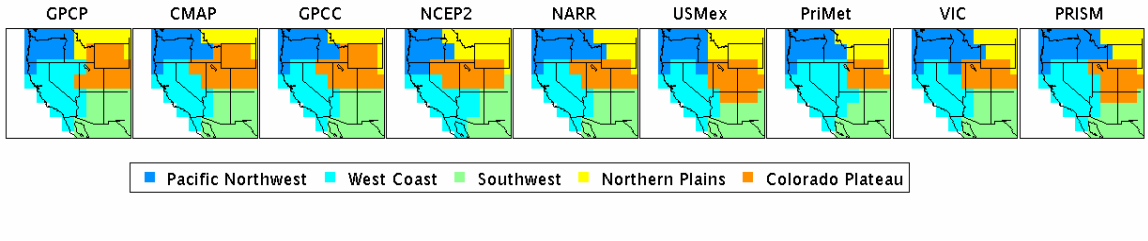

Figure 3. Results of the PC-based regionalization for each of the nine precipitation datasets listed in Table 1.

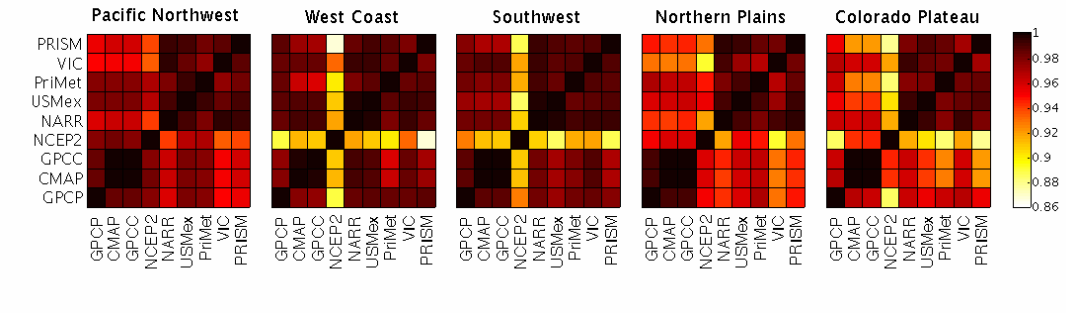

Figure 4. Congruence coefficient representing the degree of likeness between loading patterns for each pair of datasets (Table 1) and for each region shown in Figure 3.

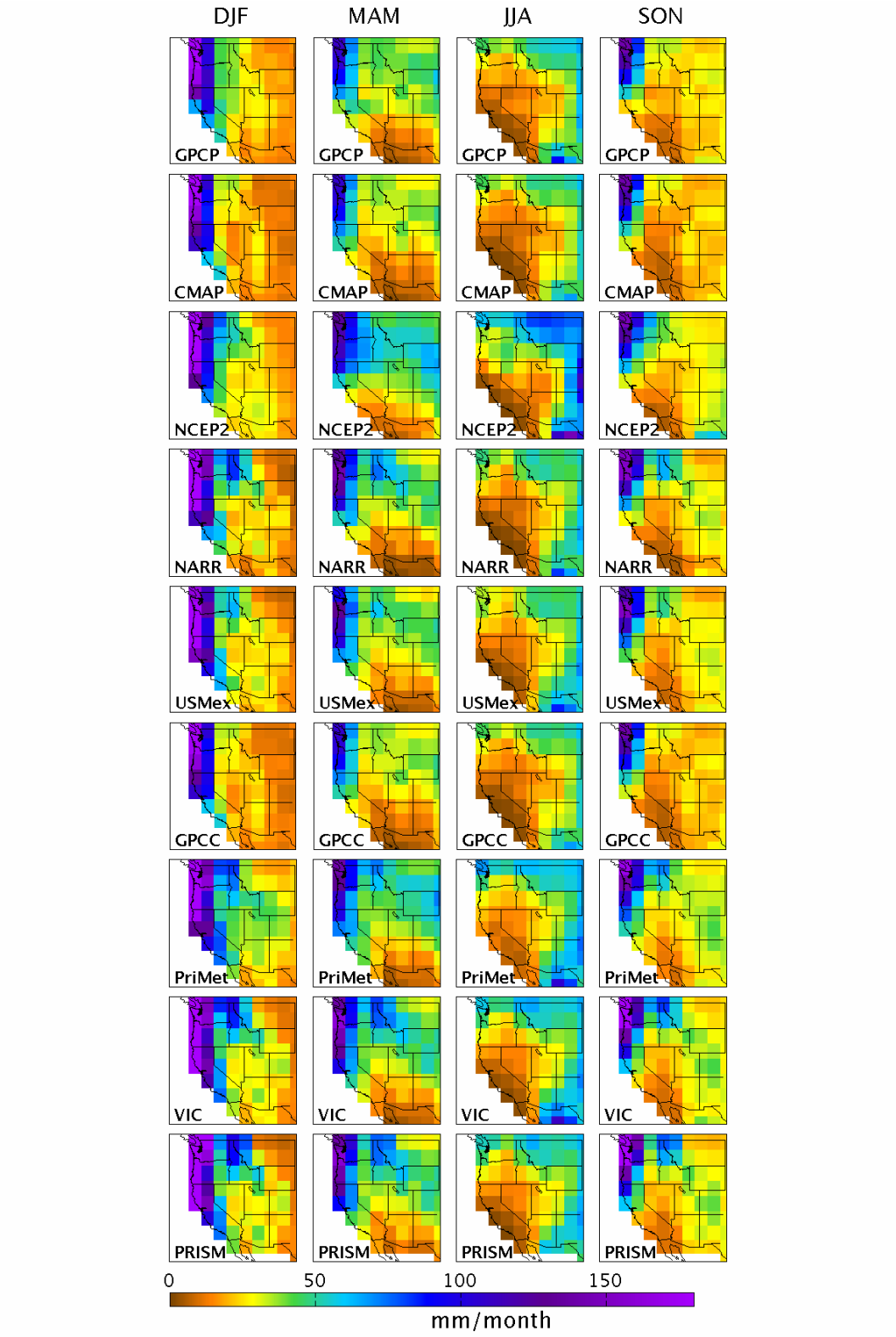

Figure 5. Long-term seasonal precipitation for December-February (DJF), March-May (MAM), June-August (JJA), and September-November (SON).

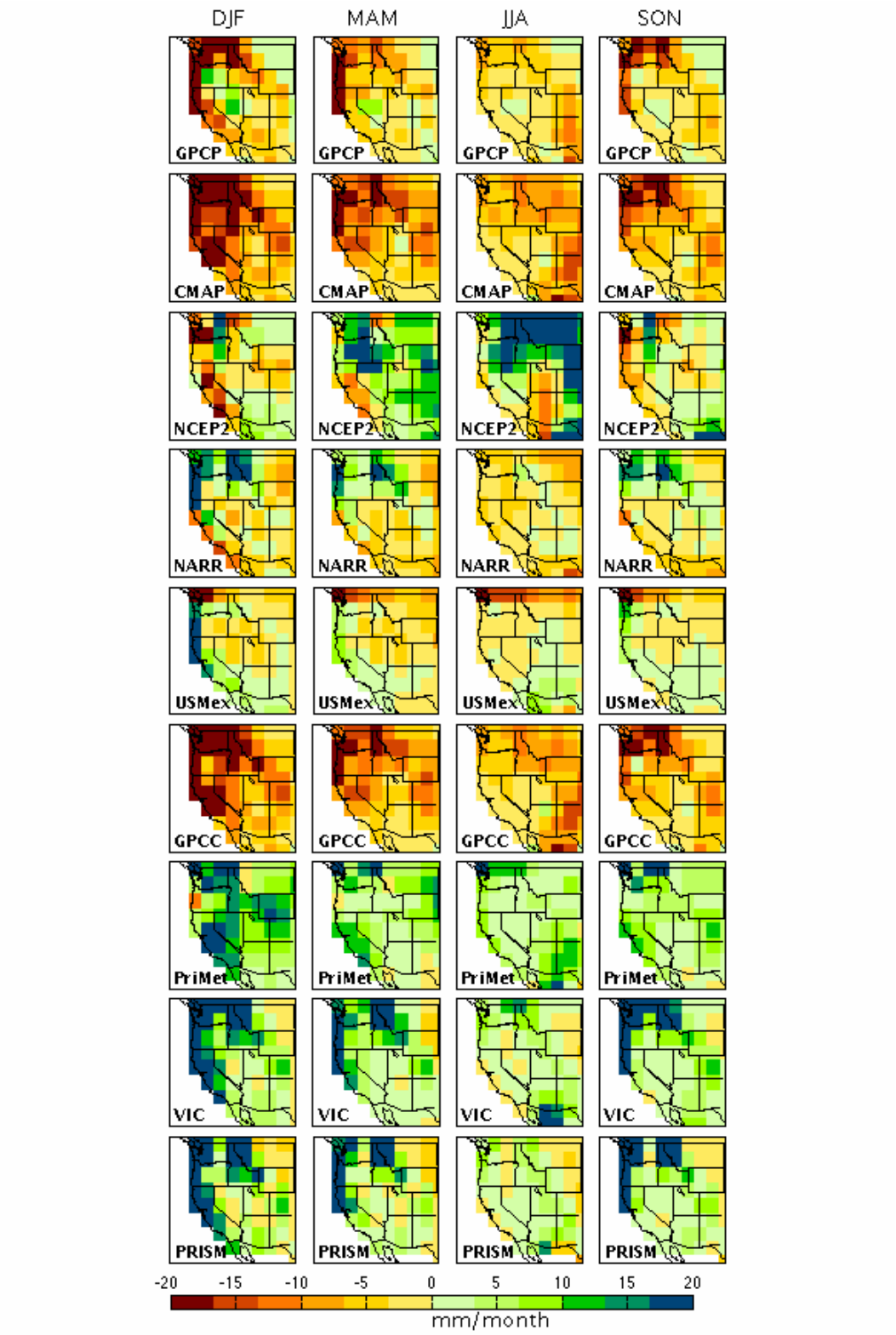

Figure 6. Difference from ensemble long-term (1/1986-7/2000) seasonal mean precipitation. The ensemble is created by taking the average over all datsets for each grid cell.

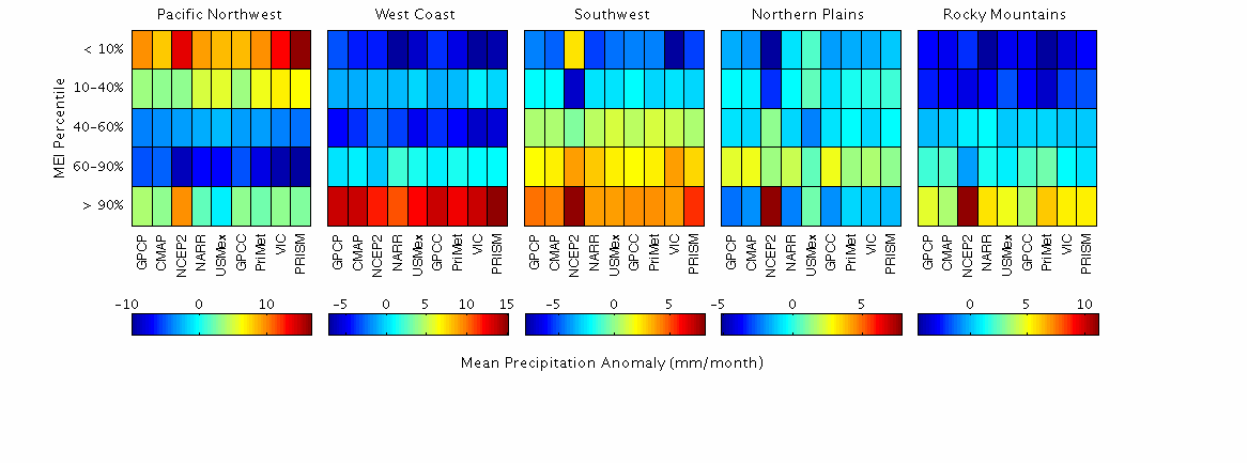

Figure 7. Average precipitation anomaly for varying strengths of ENSO using percentile of the Multivariate ENSO Index.

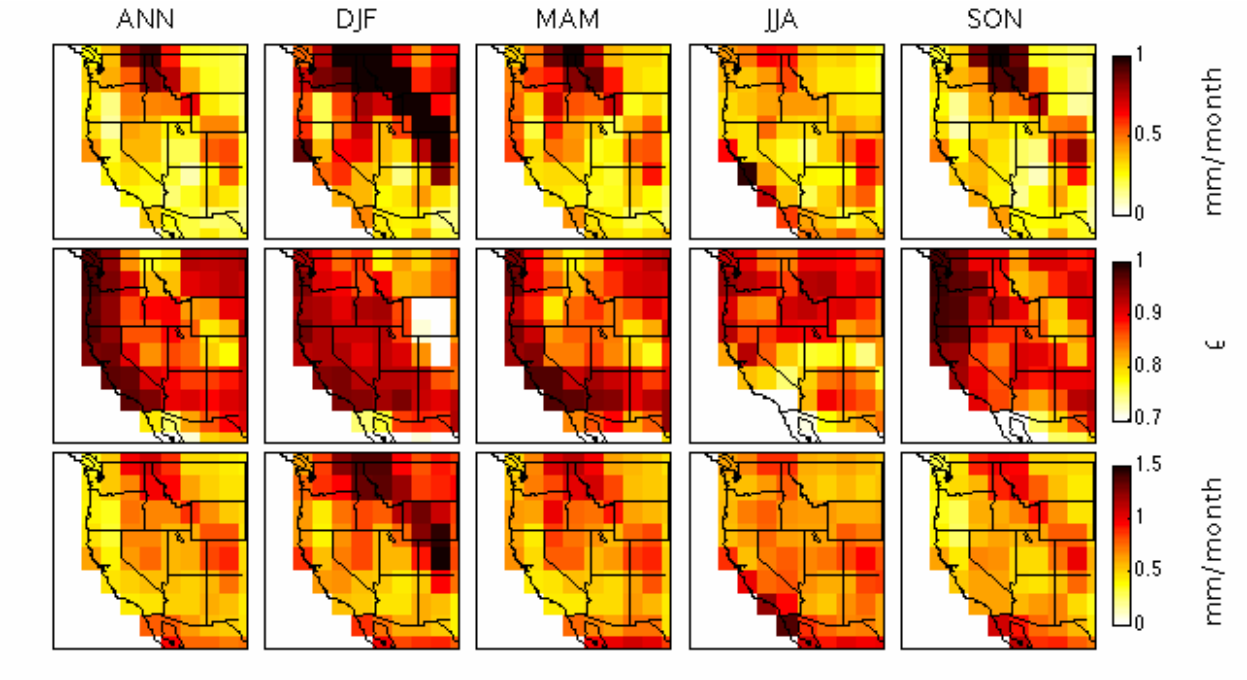

Figure 8. Average RMSE (bottom), correlation (middle) and normalized absolute value of bias (top) between data pairs for winter (DJF), spring (MAM), summer (JJA), fall (SON), and all seasons (ANN).